

An Actuated Gaze Stabilization Platform for a Flapping-Wing Microrobot

Sylvain Mange¹, E. Farrell Helbling², Nick Gravish^{2,3}, and Robert J. Wood²

Abstract—Active damping of sensor inputs may reduce the computational requirements for robot locomotion. Power-reduction in micro-robotics is extremely important given current limitations of onboard power supplies, such as batteries. In this paper we design and fabricate a camera stabilization system for a micro-aerial vehicle (MAV). Our system mechanically stabilizes an onboard camera carried on a 80 mg MAV. We describe the challenges of micro-scale actuation of these systems and demonstrate on-board stabilization of vision during flight.

I. INTRODUCTION

Microrobots are rapidly advancing in locomotor capabilities, driven in large part by fabrication advances [1]. However, a critical challenge in microrobotics remains in the integration of onboard sensory and computational capabilities. Current limitations in battery technology make long range locomotion with a full suite of onboard sensors highly impractical. A possible method to reduce power costs in microrobotic locomotion may be to provide mechanical “pre-processing” of computationally intensive sensors through low-power active mechanical damping. Active and passive mechanical systems can thus provide a first layer towards cleaning sensor data and reduce uncertainty and computational load from processing sensory inputs.

A fundamental goal of micro-aerial vehicles (MAVs) is stable, guided flight through onboard control and sensor systems. Vision-based sensors are important aspects of flight control and many studies of vision based navigation on larger aerial vehicles have been demonstrated [2], [3]. A challenge in vision-based flight control (on short timescales) and localization (on longer timescales) is the calculation of self-movement through optic flow and feature detection despite inherent camera noise and unstable body rotations. The computational requirements for optic flow and feature detection algorithms are high [4], and these systems are not necessarily robust to rapid body movements.

The RoboBee is an 80 mg flapping-wing micro-aerial vehicle which is capable of controlled and sustained flight [5], [6]. Flapping-wing flight is inherently unstable and thus requires robust control systems and sensors to maintain stable locomotion [7], [8]. Six degree of freedom flight control is generated through synchronous and asynchronous actuation

¹Sylvain Mange is with the School of Engineering, Ecole Polytechnique Fédérale de Lausanne, Lausanne, Switzerland sylvain.mange@alumni.epfl.ch

²EFH, NG, and RJW are with the School of Engineering and Applied Sciences and the Wyss Institute for Biologically Inspired Engineering, Harvard University, Cambridge, MA, USA. rjwood@seas.harvard.edu

³Current affiliation is Univ. Calif. San Diego, Mechanical & Aerospace Engineering Dept., San Diego, CA, USA

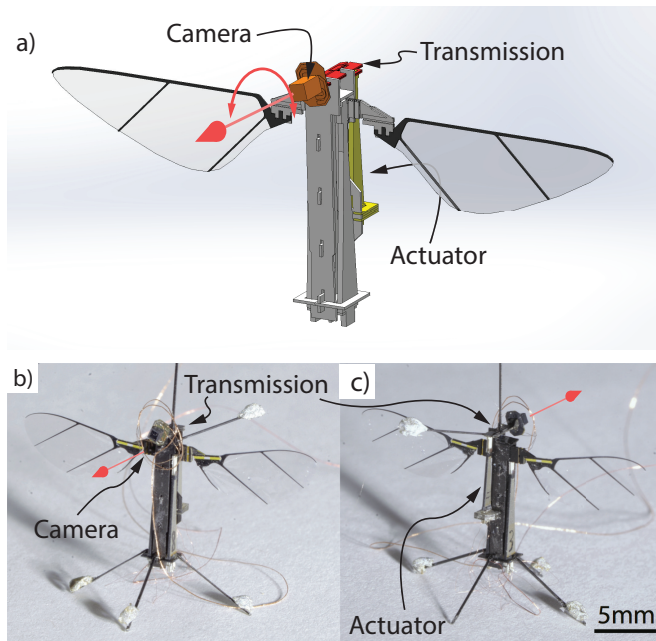


Fig. 1. a) Concept of image stabilization mechanism. b-c) Forward and reverse view of RoboBee with camera mounted stabilization system.

schemes for the left and right wings. Previously we have demonstrated that the RoboBee is capable of vision-based control of altitude [9]. However, a limitation of optic flow based control is that movements measured through optic flow require decoupling self-rotation, self-translation, and the high-frequency self-vibration from the flapping wings.

Active sensor systems, combinations of active mechanisms and a sensor package, may be able to “pre-process” sensor inputs to reduce input noise to control systems. For instance, the cell-phone industry has propelled the development of active camera stabilization systems, which are now commonly found in commercial smart phones. However, these systems are highly specialized and limited in their range of motion and thus cannot provide the angular displacements necessary for RoboBee flight. However, similar design and fabrication methods as used to manufacture the RoboBee structure, transmissions, and actuators may be used to design and integrate an onboard vision stabilization system for the RoboBee.

In this paper we propose and develop a micro-fabricated active vision sensor system using an off the shelf 3.1 mg camera with 250×250 resolution (NanEye 2D, AWAIBA) and a custom gaze stabilizer. We employ the PC-MEMS

design and fabrication methodology to construct a rotation stabilizer to compensate for roll rotations perceived by a head-mounted camera. The requirements of low-mass, high-bandwidth, and high angular displacement on this stabilizer present significant design challenges at this small scale. We discuss in this paper the design, fabrication, and demonstration of an on-board 27 mg gaze stabilization system to augment and enhance vision-based guidance and control in insect-scale MAVs.

II. STABILIZER DESIGN

Sensors for control and navigation must be mounted onto the microrobot for future autonomous navigation and stability. Previous Robobee sensors such as gyroscopes [10], magnetometers [11], and light sensors [12] have been rigidly mounted to the airframe. The active stabilization system described here presents additional challenges to Robobee integration because it must have a low mass to meet the payload capacity of the vehicle, a small footprint to not interfere with the wing and actuator motions, and a clear line of sight to be useful as a vision sensor. The size and mass demands of this sensor required the design of a custom actuator and transmission platform for the camera to be mounted on (Fig. 2).

A. Transmission

1) *Design and Fabrication:* We used PC-MEMS based design and manufacturing for the camera stabilization system [13]. This fabrication process is capable of making lightweight mechanisms and is used for the fabrication of the Robobee [5]. To minimize complexity of the camera rotation mechanism we used a simple four-bar linkage design for the rotation transmission, with hinges made of flexible layers linked by planar pieces made of rigid layers (Fig. 3). This transmission is similar to that used in the RoboBee’s wing actuation, although the lower transmission ratio permits less material needed. We maximized the transmission ratio to give maximum output angle with minimum required linear input motion. However, practical fabrication considerations require that structural material separate the two serial flexure layers (Fig. 3), and thus this link cannot be made smaller than $500\ \mu\text{m}$.

A workaround is to have consecutive hinges next to another as shown on Fig. 3b. The simplest way to create flexure hinges with the PC-MEMS process is to sandwich a flexible layer between two rigid layers; a gap in the rigid layers forms a hinge. This simple layout causes all hinges to be in the same plane when at rest. From this position, regardless of the hinge layout, having the actuator move perpendicularly with respect to the plane would cause limited rotations of the hinges. Larger rotations are produced if a link is instead moved along the plane, but this results in a singularity in the resting position. To avoid this, we offset one of the hinges onto another flexible layer, creating a second plane (Fig. 3c). The motion of the final transmission design can be seen in Fig. 3d.

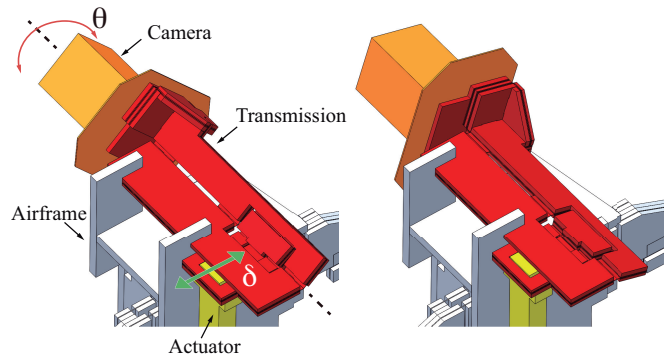


Fig. 2. The complete transmission (red) and camera (orange) mounted on the airframe (gray). The actuator tip (yellow) undergoes lateral displacements, δ , producing camera rotation θ .

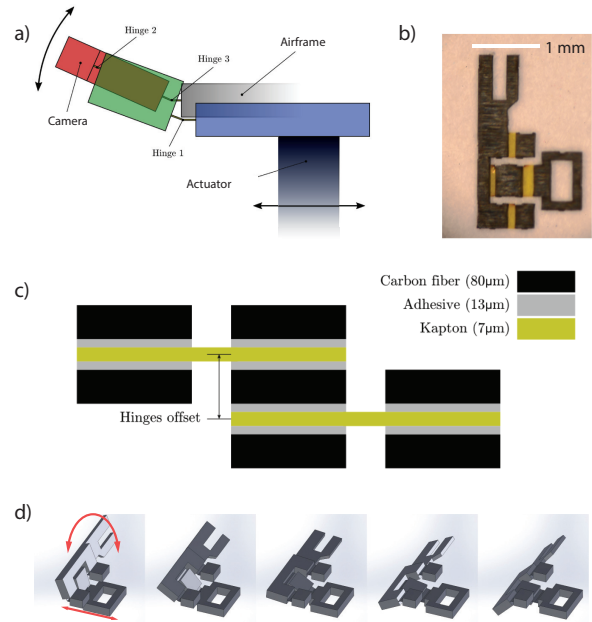


Fig. 3. Camera stabilization transmission. a) Schematic of four-bar transmission with linear actuator input and camera rotation. b) Fabricated transmission. c) Layout details of transmission. d) Transmission motion.

As the size of the link approaches the length of the flexure hinges, the fact that flexure hinges are not exact revolute joints and are subject to buckling starts to create appreciable errors with respect to the desired trajectory. As discussed above, all hinges are in the same plane at rest and the input part is then actuated along an in-plane direction, amplifying the buckling issue. An efficient solution is to use castellated hinges, which greatly reduce the hinges length [14]. Figure 2 shows the complete transmission.

B. Actuator

Actuating a mechanism onboard an 80 mg flying robot is a challenge in itself, primarily because of the limited weight and size budget that this implies. The small size precludes the use of typical electromagnetic motors. Other actuators, such as dielectric elastomers, require voltages in

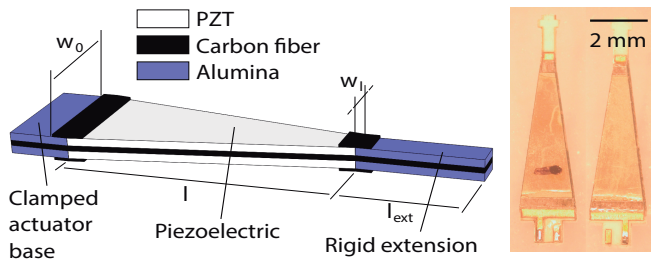


Fig. 4. Actuator design (left) and a realized actuator (right)

the kilovolt range, creating challenges for onboard high voltage generation without adding prohibitive electronics weight. Electrostatic actuators can be scaled down to MEMS-scales; however, the most compatible actuation method is piezoelectric cantilever actuators [15]. An piezoelectric actuator with a mass of 25 mg can provide approximately $200\mu\text{m}$ of tip to tip displacement at frequencies above 100 Hz with additional force than what is required for the small sensor [5].

The actuators described here are based on recent design and fabrication optimizations for piezoelectric bimorphs [16]. To achieve desired weight and size goals, the active length of the actuator, l (see Fig. 4), was reduced from 9 mm to 6 mm. The extension ratio was kept at $1/3$; increases result in marginal energy gain while adding significant weight. We chose to maintain a tip width, $w_l = 0.5\text{ mm}$ to maintain stiffness for power transmission. The low-inertia platform of the system requires less force to actuate than a standard RoboBee wing-transmission system. We therefore decided to reduce the width of the base to 1.25 mm to reduce mass.

The measured actuator displacement, δ , was slightly less than the desired goal likely due to small errors in fabrication. The actuator had a peak to peak free tip displacement of $\delta = 416\mu\text{m}$ at a drive voltage of 300 V. The frequency response was measured to be constant up to 250 Hz. The actuator for our gaze stabilization platform weighed 14.4 mg, 53% of the total stabilization sensor package.

C. Results

The transmission is able to produce an output angle of $+64^\circ$ in one direction and -57° in the other, which corresponds to actuator tip displacements of respectively $+161\mu\text{m}$ and $-175\mu\text{m}$. Figure 5 shows the frequency response of the system alone and with a dummy weight mimicking the inertia of the NanEye camera. In both cases, the response is constant until at least 60 Hz, indicating a resonant frequency beyond the frequencies of interest.

III. BENCHTOP TESTING

The RoboBee has limited payload capacity and strict geometric constraints. We selected a vision sensor (NanEye 2D, AWAIBA) with a mass of 3.1 mg and a package size of $1\times 1\times 1.7\text{ mm}^3$. This sensor offers a resolution of 250×250 pixels, a field of view of 120° , and a four-wire power and communication connection. This makes it ideal

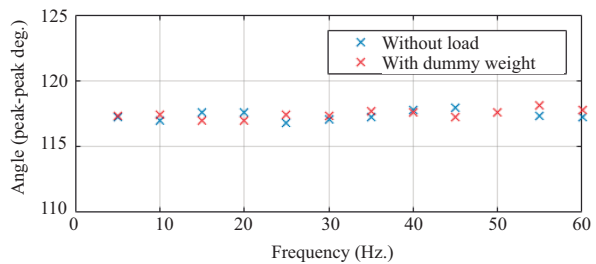


Fig. 5. Transmission frequency response. The blue points show the peak to peak output angle range as the actuator was only driving the transmission. For the red points, a dummy camera weight corresponding to the NanEye inertia was mounted on the platform.

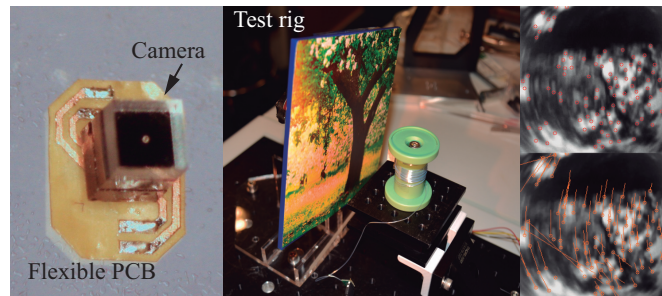


Fig. 6. a. NanEye camera module soldered on a flexible PCB. b. Benchtop test rig with natural scene. Camera is held in wire-spool. c. Two consecutive frames of the dataset showing features (top) and optic flow (bottom).

for integration on the RoboBee given its small size, reasonably high resolution, and easy hardware interfacing. We mounted the camera on a flexible printed circuit board ($25\mu\text{m}$ copper, $12.5\mu\text{m}$ polyimide) to minimize weight (Fig. 6). An additional tether for camera power and communication was routed off the RoboBee to an FPGA board (NanEye USB 2.0, AWAIBA), sending real-time vision information to an offboard computer.

A. Rotation detection

As a proof of concept, we demonstrate that the stabilization platform could be an independent system, with the vision sensor providing rotation estimation for a closed-loop controller. In addition, this reduces the need for additional sensors to measure angular velocity, such as a gyroscope or magnetometer, which would increase the payload of the robot. It is also motivated by the fact that head stabilization on some flying insects is controlled by visual information [17]. We incorporated optic flow algorithms to compute the camera rotation about the focal axis.

We built an experimental setup to develop and test the algorithm, where the camera is fixed in place and pointed at a rotating scene that covers its whole field of view, thus simulating camera rotations (Fig. 6). We mounted an image of a natural scene to a rotation stage and measured the rotation scene with a potentiometer for a ground truth measurement. Datasets were acquired with the scene rotating at up to two revolutions per second with the camera in the following three configurations:

- (a) still, pointing at the scene center
- (b) moved to the right at 4 cm/s
- (c) moved backwards at 4 cm/s.

Additionally, a dataset (d) was captured with the camera pointing at the side of the scene, which results in faster optic flows. An example of two consecutive frames from the dataset (a) is shown in Fig. 6b.

Since only one global motion for the whole scene needs to be extracted, and in order to limit computational cost, sparse optical flow was chosen and computed with the Lukas-Kanade method with pyramids [18]. A number of steps need to be performed prior to applying the optic flow algorithm. First, grayscale frames are smoothed using a median filter to reduce the effect of sensor noise while keeping edges and distinctive features. Then feature points need to be selected on the first frame for the optic flow algorithm to match to the subsequent frame. Multiple methods that can find features have been published, and three fast methods were compared. Table I shows the results of feature detection with the three algorithms across the datasets.

TABLE I
COMPARISON OF METHODS FEATURE DETECTION

	Datasets (a)-(c)	Dataset (d)
Shi & Tomasi's algorithm [19]	92 %	57 %
FAST (Features from Accelerated Segment Test) [20]	89 %	72 %
AGAST (Adaptive and Generic Accelerated Segment Test) [21]	91 %	72 %

The chosen solution is to use Shi & Tomasi's algorithm, and to additionally run FAST when not enough features are found. Since the detected features are corners, a refinement step of the feature positions can then be performed using the image gradient in the neighborhoods of the features. Next, the Lukas-Kanade method matches the features to points on the subsequent frame, yielding a vector field of flows. Lastly, an affine transform (constrained to include no shear), is fitted on this vector field using a least-squares approach. This affine transform holds the rotation angle around the optical axis.

B. Integration with the RoboBee

The RoboBee used in these experiments is mechanically similar to the robot presented in [16], with slight modifications to the airframe to accommodate the stabilizer (see Fig. 1). The stabilizer's piezoelectric actuator was grounded to the back wall of the airframe, with the transmission system linking to the camera over the top of the airframe. Once the stabilizer was attached to the airframe, we visually aligned the camera to the vertical surface of the transmission. We used 44 gauge copper wire for camera power and communication, the wire gauge was selected to allow for communication to the sensor without adding stiffness which would prevent camera rotation. To decrease stiffness further,

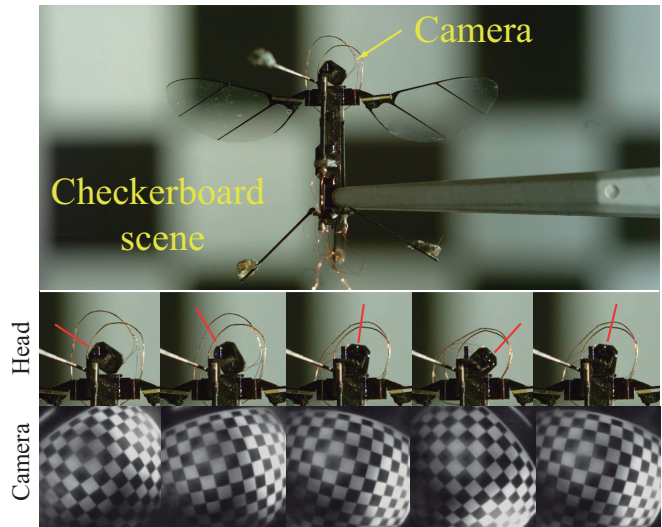


Fig. 7. Open loop testing of camera motion mounted on RoboBee.

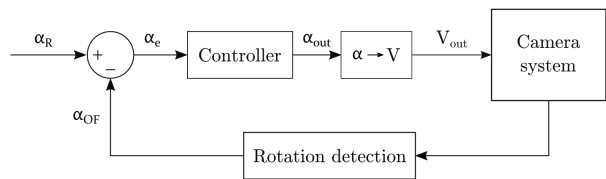


Fig. 8. a) Optic-flow based stabilization testing. a) Two consecutive frames of the dataset.

we looped the wires around the camera for two and half rotations before they were strain relieved to the airframe. With the wires, we saw a slight decrease in output range from -57° – 64° to -41° – 60° (Fig. 7). The developed camera stabilization system adds 27mg to a RoboBee, well within the payload capacity of the vehicle, 170 mg [16].

C. Preliminary Control Test

To test the feasibility of the stabilizer as a stand-alone device, we first measured the rotation angle from the optic flow computation of the camera images (see Fig. 7). The frames of the images are sent through the camera tether to the USB FPGA acquisition board (CMOSIS) and recorded using their API. This program also computes the measured angular position of the camera. This angle is then sent over serial (RS232) to an xPC Target system (Mathworks), which uses this position as the input to the stabilizer's controller.

The control for the stabilizer can be seen in Fig. 8. Because the desired angle is always zero (no rotation) the error input on the PID controller is just the measured optical flow angle, α_{OF} . The controller seeks to minimize this angle by applying a voltage to the piezoelectric actuator. The mapping between angle and actuator drive signal was experimentally determined to be a linear transformation $V_{out} = 3\alpha_{out}$. Because we don't want to generate any large acceleration that could damage the actuator or the transmission, and also because we want to use the mechanical system in the linear part of its frequency response, a low-pass filter is added after

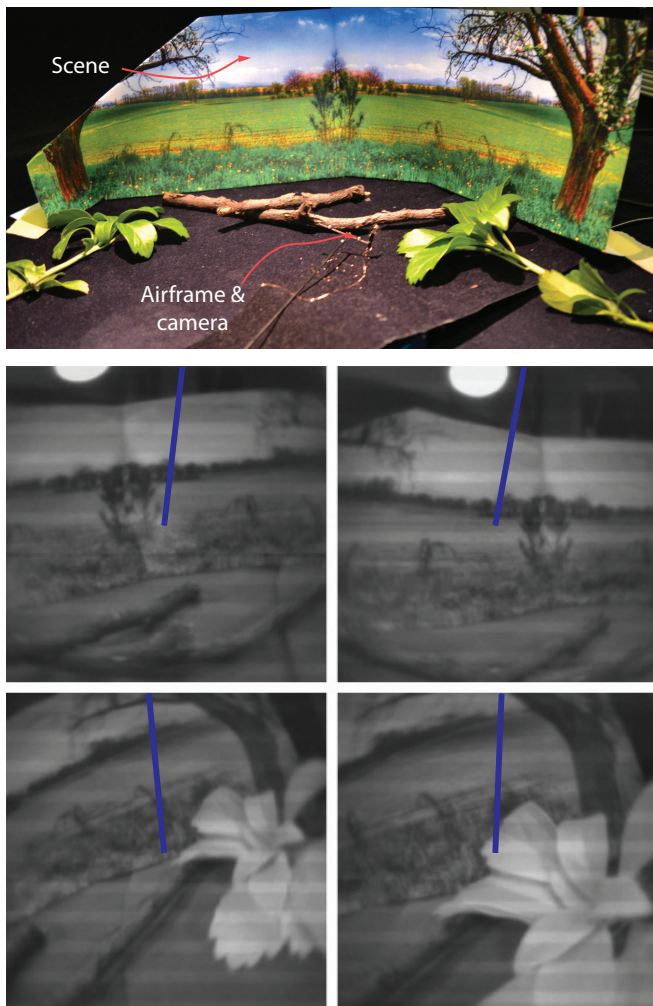


Fig. 9. a) Scene with 3D topography and natural images. a) Consecutive frames of the dataset showing stabilized video and robot rotation angle (blue line).

the proportional controller. This filter was designed with a cutoff frequency of 40 Hz in order to match the measured frequency response shown in Fig. 5, we also assume that the step size of the measured angles is small. This voltage was then sent through a high voltage amplifier and sent to the camera actuator. The controller gains were hand-tuned. This entire process is performed at approximately 45Hz.

We mounted the airframe of the robot to the end of a wand with a series of motion capture markers. The position and orientation of the wand (and therefore the airframe) was recorded with motion capture cameras and tracking software and sent over serial to the xPC Target system. This could be used as a ground truth reference for the roll rotation of the vehicle during tests (see Fig. 9).

We created a natural-looking scene to simulate a real-world flight visualization. We manually moved the robot airframe while closed-loop control was implemented on the stabilizer. Example frames captured by the camera are shown in Fig. 9. In addition, we compared the rotations measured in the camera and those recorded in the motion capture

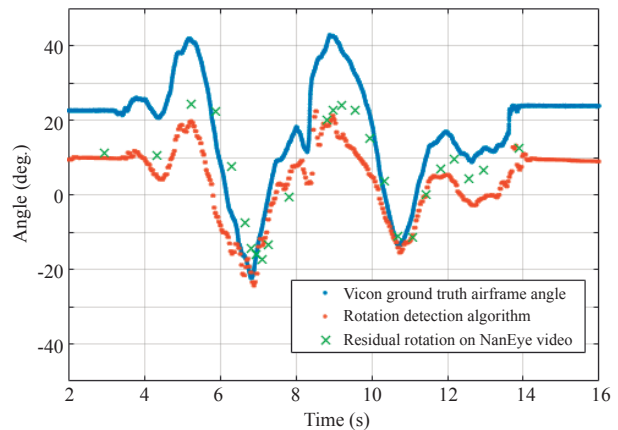


Fig. 10. Results from optic flow based stabilization.

software and we can demonstrate that some stabilization was successfully achieved (see Fig. 10).

IV. CONCLUSION

Mechanical pre-processing of sensors can reduce the computational demands for control, localization, and navigation in robot movement. Here we describe an active stabilization system for mechanical pre-processing of camera sensor data on an 80 mg flapping wing robot. The design constraints for MAVs are challenging in that the combined sensor and actuator package must be lightweight to merit use, and must integrate into a robot with very little available space. Using PC-MEMS based fabrication we demonstrate that a 27 mg vision stabilization integrated into the RoboBee can act to help stabilize the visual signal from a camera under small-angle perturbations.

One goal of active mechanical pre-processing is to use low-power, high-bandwidth sensor data to stabilize a high-power, low-bandwidth sensor. In this paper we demonstrated the feasibility of this approach, however we did not implement the full control-loop of using a low-power, high-bandwidth onboard sensor to stabilize the on-board camera. Previous experiments have demonstrated that sensor packages such as artificial ocelli, accelerometers, and magnetometers can be carried onboard in controlled flight and even used directly for feedback control. The integration of onboard sensors to stabilize onboard active mechanical pre-processing systems remains the next challenge towards autonomous flight of MAVs and mechanical pre-processing of visual information may aid this goal.

A secondary goal of the visual gaze stabilization platform developed here is to explore the feasibility of using vision information to stabilize vision sensors. Fast, closed-loop optic flow based gaze stabilization may simplify the design of higher level localization and flight stabilization controllers. We demonstrated that optic flow based methods can reduce camera roll for the slower motions of a hand actuated Robobee. Flight with onboard optic flow stabilization remains an open challenge for future work; to integrate more

robust optic flow tracking with faster cameras towards true optic flow based gaze stabilization on an insect-scale robot.

ACKNOWLEDGMENTS

This work was partially supported by the National Science Foundation (award #IIS-1514306) and the Wyss Institute for Biologically Inspired Engineering. Any opinions, findings, and conclusions or recommendations expressed in this material are those of the authors and do not necessarily reflect the views of the National Science Foundation.

REFERENCES

- [1] J P Whitney, P S Sreetharan, K Y Ma, and R J Wood. Pop-up book MEMS. *J. Micromech. Microeng.*, 21(11):115021, 2011.
- [2] J C Zufferey and D Floreano. Fly-inspired visual steering of an ultralight indoor aircraft. *IEEE Trans. Rob.*, 22(1):137–146, February 2006.
- [3] G C H E de Croon, K M E de Clercq, Ruijsink, Remes, and C de Wagter. Design, aerodynamics, and vision-based control of the DelFly. *International Journal of Micro Air Vehicles*, 1(2):71–97, 2009.
- [4] G C H E de Croon, C De Wagter, B D W Remes, and R Ruijsink. Sub-sampling: Real-time vision for micro air vehicles. *Rob. Auton. Syst.*, 60(2):167–181, 2012.
- [5] Kevin Y Ma, Samuel M Felton, and Robert J Wood. Design, fabrication, and modeling of the split actuator microrobotic bee. In *2012 IEEE/RSJ International Conference on Intelligent Robots and Systems*, pages 1133–1140. IEEE, 2012.
- [6] Kevin Y Ma, Pakpong Chirarattananon, Sawyer B Fuller, and Robert J Wood. Controlled flight of a biologically inspired, insect-scale robot. *Science*, 340(6132):603–607, 2013.
- [7] Pakpong Chirarattananon, Kevin Y Ma, and Robert J Wood. Adaptive control of a millimeter-scale flapping-wing robot. *Bioinspir. Biomim.*, 9(2):025004, June 2014.
- [8] Wei Shyy, Chang-Kwon Kang, Pakpong Chirarattananon, Sridhar Ravi, and Hao Liu. Aerodynamics, sensing and control of insect-scale flapping-wing flight. *Proc. Math. Phys. Eng. Sci.*, 472(2186):20150712, February 2016.
- [9] Pierre-Emile J Duhamel, Castor O Perez-Arancibia, Geoffrey L Barrows, and Robert J Wood. Biologically inspired optical-flow sensing for altitude control of flapping-wing microrobots. *IEEE/ASME Transactions on Mechatronics*, 18(2):556–568, 2013.
- [10] Sawyer B Fuller, E Farrell Helbling, Pakpong Chirarattananon, and Robert J Wood. Using a mems gyroscope to stabilize the attitude of a fly-sized hovering robot. In *IMAV 2014: International Micro Air Vehicle Conference and Competition 2014, Delft, The Netherlands, August 12-15, 2014*. Delft University of Technology, 2014.
- [11] E F Helbling, S B Fuller, and R J Wood. Pitch and yaw control of a robotic insect using an onboard magnetometer. In *2014 IEEE International Conference on Robotics and Automation (ICRA)*, pages 5516–5522, May 2014.
- [12] Sawyer B Fuller, Michael Karpelson, Andrea Censi, Kevin Y Ma, and Robert J Wood. Controlling free flight of a robotic fly using an onboard vision sensor inspired by insect ocelli. *J. R. Soc. Interface*, 11(97):20140281, 6 August 2014.
- [13] JP Whitney, PS Sreetharan, KY Ma, and RJ Wood. Pop-up book mems. *Journal of Micromechanics and Microengineering*, 21(11):115021, 2011.
- [14] RJ Wood, S Avadhanula, R Sahai, E Steltz, and RS Fearing. Micro-robot design using fiber reinforced composites. *Journal of Mechanical Design*, 130(5):052304, 2008.
- [15] RJ Wood, E Steltz, and RS Fearing. Optimal energy density piezoelectric bending actuators. *Sensors and Actuators A: Physical*, 119(2):476–488, 2005.
- [16] Noah T Jafferis, Moritz A Graule, and Robert J Wood. Non-linear resonance modeling and system design improvements for underactuated flapping-wing vehicles. In *2016 IEEE International Conference on Robotics and Automation (ICRA)*, pages 3234–3241. IEEE, 2016.
- [17] R Hengstenberg. Stabilizing head/eye movements in the blowfly calliphora erythrocephala. *The Head-Neck Sensory Motor System*, pages 49–55, 1992.
- [18] Jean-Yves Bouguet. Pyramidal implementation of the lucas kanade feature tracker. In *Intel Corporation, Microprocessor Research Labs*, 2000.
- [19] Jianbo Shi and Carlo Tomasi. Good features to track. In *Computer Vision and Pattern Recognition, 1994. Proceedings CVPR'94., 1994 IEEE Computer Society Conference on*, pages 593–600. IEEE, 1994.
- [20] Edward Rosten and Tom Drummond. Machine learning for high-speed corner detection. In *European conference on computer vision*, pages 430–443. Springer, 2006.
- [21] Elmar Mair, Gregory D Hager, Darius Burschka, Michael Suppa, and Gerhard Hirzinger. Adaptive and generic corner detection based on the accelerated segment test. In *European conference on Computer vision*, pages 183–196. Springer, 2010.